Oceanic Zircon as a Petrogenetic Indicator

L.Ya. Aranovich✉, N.S. Bortnikov, A.A. Borisov

Institute of Geology of Ore Deposits, Petrography, Mineralogy, and Geochemistry, Russian Academy of Sciences,
Staromonetnyi per. 35, Moscow, 119017, Russia

Abstract—We present results of a study of the morphology, internal structure, and chemical composition of oceanic zircon, which show that zircon is a sensitive indicator of tectonic and physicochemical processes occurring in the lower oceanic crust. Crystallization of magmatic zircon in gabbroids is not an instantaneous process; it proceeds in the course of differentiation of parental melts in the tectonically active mid-ocean ridge (MOR) setting. The main geochemical indicator of crystallization differentiation during magma cooling is an increase in Hf content toward the zircon grain edge. Zoning is also observed in magmatic zircons from oceanic plagiogranites (OPG), but it is weaker, apparently because of the narrower temperature range of zircon crystallization in these rocks. The OPG zircons are depleted in REE as compared with the least altered magmatic zircons of gabbro, which is probably due to the formation of OPG during the partial melting of gabbro with the participation of concentrated water–salt fluid, a derivate of seawater, and due to the co-crystallization of zircon and apatite. High-temperature hydrothermal processes within slow-spreading MORs lead to a partial or complete recrystallization of zircon as a result of dissolution/redeposition. A significantly reduced cerium anomaly and the presence of microinclusions of xenotime, uranium and thorium oxides or silicates, and, sometimes, baddeleyite in zircon alteration zones indicate a reducing type and high alkalinity of the hydrothermal fluid. The fluid, a derivate of seawater, acquires these features during circulation near the axial zone of ridges as a result of phase separation in the system H_2O–NaCl and interaction of the fluid with abyssal peridotites of oceanic core complexes. The estimated solubility of zircon in basic melts indicates that even near-solidus crystallization of zircon is highly unlikely in anhydrous basaltic melts but is possible in differentiates of deep-seated hydrous basic magmas. The Ti-in-Zrn geothermometer must be used with caution, because variations in the Ti content in zircon might be controlled not only by temperature but also by other factors, especially when mineral inclusions in zircon testify to a drastic change in its growth (dissolution) conditions. A geothermometer based on the distribution of Zr and Hf between zircon and the host rock has several advantages over indicators of the crystallization temperature of magmatic zircon that are based on the zircon saturation index and the content of Ti in zircon. It does not depend on the composition of melt and on the correct estimates of the SiO_2 and TiO_2 activity. In addition, reconstruction of the Zr and Hf fractionation trends during crystallization of zircon from granitoid melts makes it possible to evaluate the temperature of separation of more differentiated melt fractions.

Keywords: zircon, mid-ocean ridge, gabbro, plagiogranites, geothermometry

INTRODUCTION

Seventy years ago, the book "Introduction to the Mineralogy of Silicates" by Sobolev (1949) was published. It gave rise to one of the most promising fields of petrology, namely, the use of minerals of variable composition for the reconstruction of the physicochemical conditions of formation of crystalline rocks. Sobolev focused attention on the regularities of changes in the contents of major oxides in rock-forming minerals. The progress in this scientific field made it possible to design various mineral thermometers (Perchuk, 1970) and barometers (Aranovich, 1991) and to develop polymineral geothermobarometry based on calculations of equilibria with the use of thermodynamic databases for rock-forming minerals (Berman and Aranovich, 1996; Holland and Powell, 1998; Reverdatto et al., 2017).

In recent years, the introduction of local methods for geochemical and isotope analyses has shifted focus to study of the behavior of trace and rare-earth elements, primarily in accessory minerals. Zircon is one of the most interesting of such minerals. It can contain impurities of Hf, Y, P, U, Th, Sc, Nb, Ti, and REE (few ppm to 3 wt.%) and preserve them after crystallization (Harley and Kelley, 2007). This specific feature makes zircon the crucial source of information about the age and duration of geologic processes (a U–Th–Pb geochronometer), the temperatures of mineral formation, the origin and transformation of crustal rocks, and the evolution of hydrothermal fluids (Watson and Harrison, 1983; Davis et al., 2003; Hoskin and Schaltegger, 2003; Harley and Kelley, 2007; Aranovich et al., 2013, 2015; Grimes et al., 2009; 2015).

Findings of zircon in ophiolites, ancient metamorphosed oceanic rocks (Kolman, 1979), made it possible to date the main stages of geodynamic evolution of regions (Dobretsov and Zonenshain, 1985; Bogdanov and Dobretsov, 1987; Do-

✉Corresponding author.
E-mail address: lyaranov@igem.ru (L.Ya. Aranovich)

bretsov et al., 2003). The finding of this mineral in recent oceanic crustal rocks (Bortnikov et al., 2005, 2008; Grimes et al., 2009; Kostitsyn et al., 2009; Zinger et al., 2010) marked a turning point in its study because of the little knowledge of such zircons as compared with continental ones. In addition, the young age of oceanic rocks and the low contents of uranium and thorium in their zircons rule out radiation damage as a factor for structural and geochemical transformations. The aim of our research is to demonstrate that zircon composition variations can be used for the estimation of the conditions of formation of the host oceanic rocks and their evolution.

MORPHOLOGY AND GEOCHEMISTRY OF ZIRCON

Zircon is found in ocean floor rocks mainly in the sections of oceanic core complexes (OCC) widespread in slow-spreading ridges, in particular, the Mid-Atlantic Ridge (MAR). Such complexes comprise variably altered rocks of the oceanic lithosphere, mostly ultrabasic rocks and gabbroids, with scarce veins and small bodies of silica-rich feldspathic rocks, which expose at the ocean floor surface. Such felsic rocks are often called "oceanic plagiogranites" (OPG) (Coleman and Peterman, 1975; Coleman, 1977; Searle, 2013; Ciazela et al., 2015). The data reported below were obtained in studies of zircons from MAR rocks localized

within 5–13ºN (Aranovich et al., 2010, 2013, 2015, 2017; Bortnikov et al., 2008).

Figure 1 shows typical morphological varieties of zircons. **Magmatic zircons of gabbroids** are usually found as elongate xenomorphic grains (Fig. 1*a*), whereas euhedral and subeuhedral crystals with a clear zone–sectorial structure are rare in gabbroids. **Magmatic zircons of OPG** (Fig. 1*b*) are transparent colorless euhedral crystals with a smooth surface of their prisms and pyramids. They are usually more isometric than zircons from gabbroids. In cathodoluminescence (CL) images these zircons show a fine-zoned, sectorial, or heterogeneous internal structure.

Hydrothermally altered zircons. Magmatic zircons from gabbroids and OPG undergo late alterations, as evidenced from the resorption of the crystal faces resulted in colloform (or porous) structures. Even the most perfect subhedral grains with a clear oscillatory (magmatic) zoning are often replaced by porous zones at the edges (Fig. 1*c*). Some grains show a weak, if any, primary magmatic structure (Fig. 1*d*). Formation of porous aggregates and grains of zircon is usually associated with hydrothermal processes (Bortnikov et al., 2008; Grimes et al., 2009; Aranovich et al., 2010, 2013).

The main geochemical peculiarity of oceanic zircons is their similar REE patterns independently of the type of host rocks, grain morphology, and degree of secondary alterations. These zircons are characterized by a gradual increase
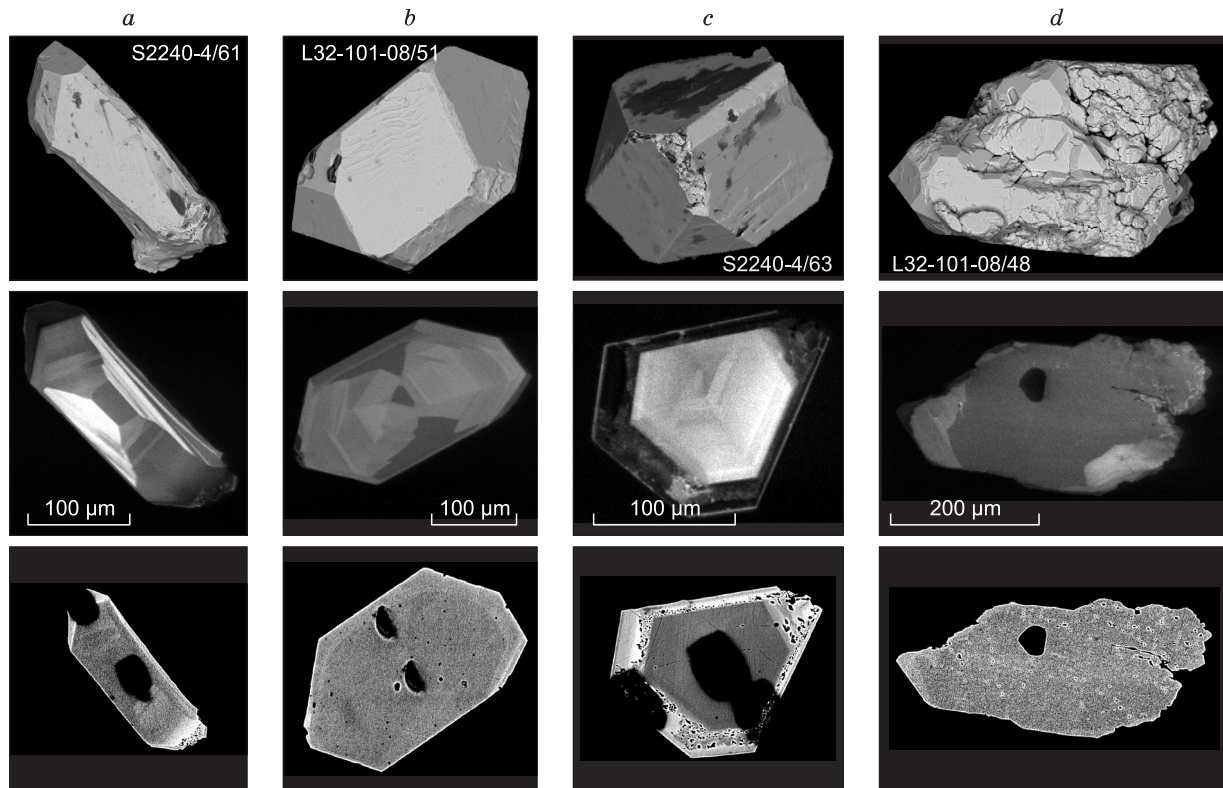

Fig. 1. The shapes (upper row), CL images (middle row), and BSE images (lower row) of zircons from MAR rocks: *a*, magmatic zircons from gabbroids; *b*, magmatic zircons from OPG; *c*, hydrothermally altered zircons from gabbroids; *d*, hydrothermally altered zircons from OPG.
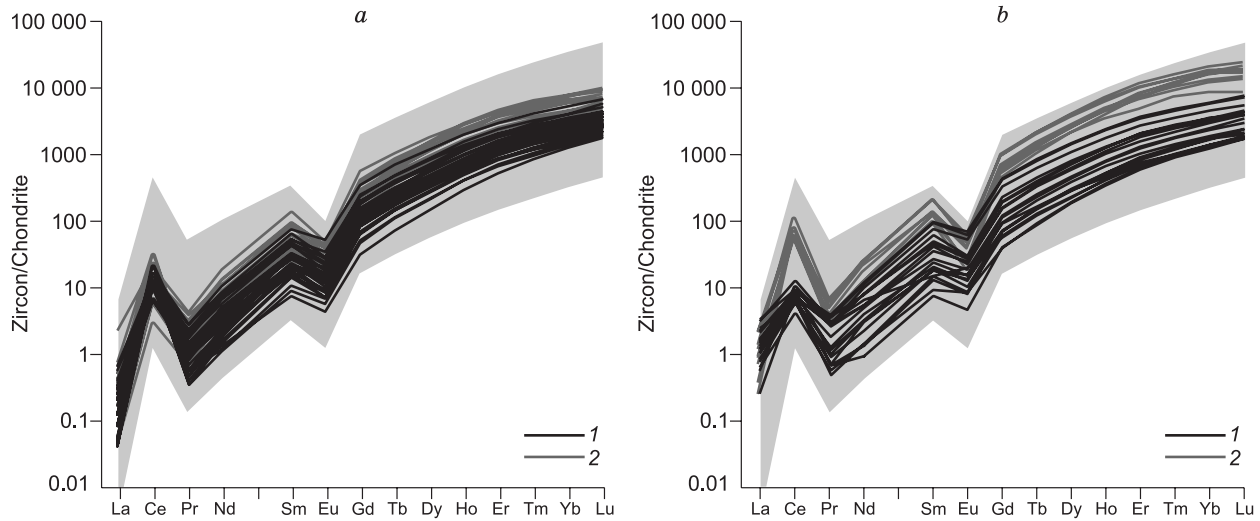
Fig. 2. Chondrite CI-normalized (McDonough and Sun, 1995) REE patterns of zircons: *a*, magmatic zircons from gabbroids (*1*) and OPG (*2*); *b*, hydrothermally altered zircons (*1*) and zircons with porous rims (*2*). Gray fields are the REE patterns of continental magmatic zircons (Hoskin and Schaltegger, 2003).

in REE contents in passing from LREE to HREE, a clear positive Ce anomaly, and a negative Eu anomaly (Fig. 2), i.e., they are similar to zircons from continental and oceanic igneous rocks (Hoskin and Schaltegger, 2003; Grimes et al., 2015). The steady REE patterns of magmatic zircons are due to their crystallochemical (energy-related) features and the absence of rock-forming minerals competing with them for Eu. The only exception is plagioclase, which crystallizes together with zircon or later and thus is responsible for its negative Eu anomaly. The REE patterns of eclogite zircons crystallized in the presence of garnet often show no negative Eu anomaly (Rubatto, 2002; Liati et al., 2009; Skublov et al., 2011). This confirms that it is plagioclase rather than the redox conditions of crystallization that is responsible for a negative Eu anomaly.

The similar REE patterns of zircons indicate that all morphological varieties of zircon crystallized from melts. However, the specifics of the magmatic stage of crystallization and postmagmatic transformations are reflected in the quantitative proportions of major isomorphic impurities, REE, and other trace elements.

Zircons from OPG veinlets often differ from the least altered zircons from the host gabbroids in lower contents of REE, especially HREE (Fig. 3). If the acid melt from which OPG zircons crystallized were the product of differentiation or dehydration melting of amphibole-containing gabbro, as suggested by Koepke et al. (2004), these zircons would be enriched in REE. The revealed REE depletion of the zircons is possible if the OPG melted from gabbroids with the participation of concentrated water–salt fluid (Aranovich et al., 2010; Silantyev et al., 2010; Pertsev et al., 2015), which can extract significant amounts of REE from granitic melts (Lukanin et al., 2010; Mannig and Aranovich, 2014). Moreover, brines extract HREE more readily than LREE (Reed et al., 2000; Mannig and Aranovich, 2014), which is observed in

our case (a negative slope of the REE patterns from La to Lu in Fig. 3).

The hydrothermally altered zircons found both in gabbro and in OPG differ from other zircons in higher contents of La and lower $(Sm/La)_N$ and Ce_N/Ce^* ratios (Fig. 4). This difference, reported by many authors (Hoskin and Shaltegger, 2003; Hoskin, 2005; Grimes et al., 2009; Kaulina et al., 2011; Aranovich et al., 2013, 2017), gives an insight into the hydrothermal fluids interacting with the rocks of the lower oceanic crust within slow-spreading ridges.

Light REE, first of all, La, could not be supplied with a fluid derived from seawater. Even under ten-fold concentration of seawater, a fluid formed during phase separation and hydration at higher horizons of the oceanic crust (Bischoff and Pitzer, 1985; Aranovich et al., 2010, 2013; Silantyev et al., 2010; Pertsev et al., 2015) can contain only a negligible amount of REE (de Baar et al., 1985). However, when reacting with the parental rocks, this fluid causes the replacement of rock-forming LREE-enriched magmatic minerals (sub-
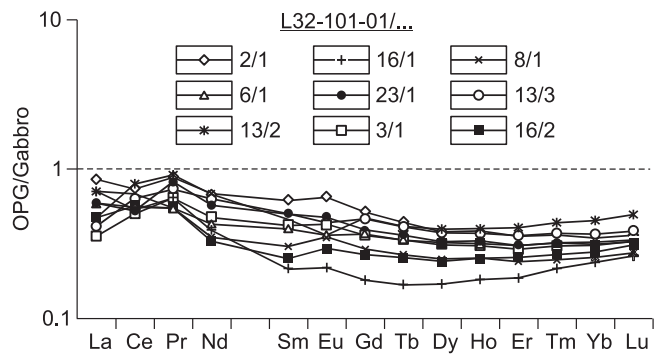

Fig. 3. REE patterns of zircons from veinlets in OPG, normalized to the average composition of the least altered grains from the host gabbroids (Aranovich et al., 2017).
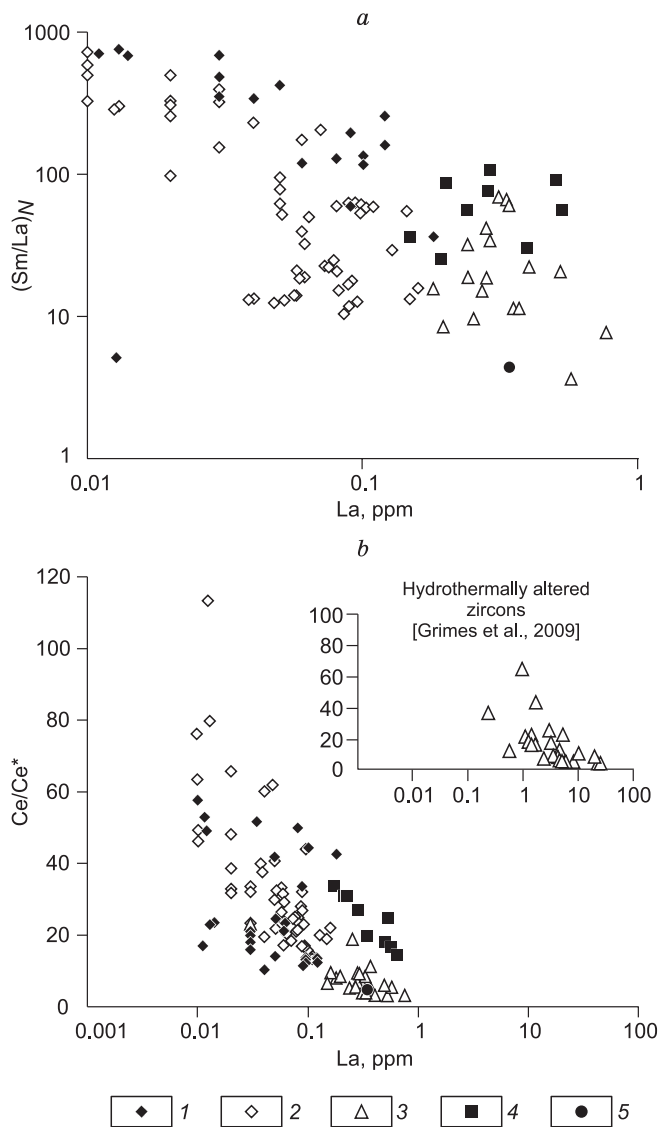
Fig. 4. Sm/La–La and Ce/Ce*–La discrimination diagrams for zircons with a magmatic internal structure. *1*, gabbro; *2*, OPG; *3*, hydrothermally altered zircons; *4*, zircons with porous rims; *5*, hydrothermally altered zircon I1028-1 (Aranovich et al., 2013). Inset shows data after Grimes et al. (2009).

calcium augite, hornblende, and basic plagioclase) by LREE-depleted hydrothermal diopside, tremolite-actinolite, and acid plagioclase (Bea, 1996; Coogan et al., 2001; Aranovich et al., 2013). Apatite, whose solubility in concentrated water–salt solutions is approximately one or two orders of magnitude higher than it is in pure water (Antignano and Manning, 2008; Manning and Aranovich, 2014), might have been an additional source of LREE.

The reduced cerium anomaly (Fig. 4) is partly due to a significant increase in the contents of neighboring elements La and Pr. Often, a decrease in the absolute content of Ce is also observed (Grimes et al., 2009; Kaulina et al., 2011; Aranovich et al., 2013, 2017). Cerium is present in the zircon structure mainly as eight-coordinated Ce^{4+}, which is

similar both in formal charge and in radius (0.97 Å) to Zr^{4+} (0.84 Å), in contrast to Ce^{3+} and other LREE. Therefore, the degree of Ce anomaly and, especially, the absolute content of Ce in zircon depend significantly on the Ce^{4+}/Ce^{3+} ratio, which, in turn, is controlled by the oxygen fugacity (Burnham and Berry, 2012; Trail et al., 2012), i.e., the redox conditions of the medium. Thus, the low Ce anomaly and Ce content in hydrothermally altered zircon indicate the reducing properties of the fluid, which it can acquire during serpentinization of abyssal peridotites widespread in OCC of slow-spreading ridges (Ciazela et al., 2015). During serpentinization of 1 mole of olivine, 1 to 2 mole of H_2O is absorbed and 0.1 to 1 mole of H_2 is released, which leads to an increase in the salinity of the fluid and in the hydrogen concentration in it (Pertsev et al., 2015). The activity of H_2 increases still more, because the H_2O–H_2 mixture shows a significant positive deviation from the ideal mixing (Aranovich, 2013), which must be still greater in the presence of NaCl.

ZIRCON-BASED GEOTHERMOMETRY

Study of zircon makes it possible to determine the age and crystallization temperature of the mineral and, in some cases, to track the thermal evolution of rocks. Three approaches to the use of zircon as a geothermometer were earlier proposed based on: (1) the bulk content of Zr in igneous rocks with known contents of major oxides (Watson, 1979; Watson and Harrison, 1983; Boehnke et al., 2013; Borisov and Aranovich, 2019); (2) the content of Ti in zircon (Watson and Harrison, 2005; Ferry and Watson, 2007); and (3) the distribution of Zr and Hf between zircon and igneous rock (Aranovich and Bortnikov, 2018).

Zircon saturation temperature of magmas. This temperature is estimated from the experimental data on the reaction of zircon (*Zrn*) dissolution/crystallization in melts (*m*) of different compositions:

$$ZrSiO_4 = ZrO_2^m + SiO_2^m. \qquad (1)$$

From the equilibrium conditions of reaction (1) it follows that

$$\ln a_{ZrO_2^m} = -\Delta G^o(1)/RT - \ln a_{SiO_2^m}, \qquad (2)$$

where $\Delta G^o(1)$ is the Gibbs free energy of reaction (1), T is the absolute temperature, R is the absolute gas constant, and a_i^m are the activities of corresponding oxides in the melt.

By statistical processing of numerous experimental data on zircon crystallization from acid melts, Boehnke et al. (2013) derived an empirical equation similar to (2):

$$\ln((Zr^m, ppm)) = 14.61 - 1.16(M - 1) - 10108/T, \qquad (3)$$

where the empirical parameter $M = (Na + K + 2Ca)/(Al \cdot Si)$ reflects variations in the melt compositions, i.e., qualitatively corresponds to the $aSiO_2^m$ variations in (2).

Recently, Borisov and Aranovich (2019) have determined the solubility of Zr in synthetic melts significantly different in composition from granites and characterized by M from 0 (absence of alkalies and Ca) to 3.5; the experiments were carried out in the temperature range 1150–1500 ºC. Processing of the experimental results and literature data (Ellison and Hess, 1986; Boehnke et al., 2013; Gervasoni et al., 2016) (129 experimental points) made it possible to derive a new equation for the solubility of Zr in silicate melts, which can be used for wide ranges of temperatures (700 to 1500 °C), melt compositions (acid to basic), and Zr concentrations (100 to 61,370 ppm):

$$\lg Zr^m \text{ (ppm)} = 4.322B - 4338.8/T(K) + 6.456, \quad (4a)$$

$$B = 0.14(X_{TiO_2}/X_{SiO_2}) + 1.3(X_{CaO}/X_{SiO_2}) + 1.5(X_{Na_2O}/X_{SiO_2}) - 4.5(X_{K_2O}/X_{SiO_2}) - 2.7(X_{Al_2O_3}/X_{SiO_2})^2 + (X_{MgO}/X_{SiO_2})^2 - 3.7(X_{CaO}/X_{SiO_2})^2 + 75(X_{K_2O}/X_{SiO_2})^2, \quad (4b)$$

where X_i are the molar fractions of oxides in the melt. Equation (4) describes the solubility of Zr in the above melts much more precisely than Eq. (3) and thus permits a more reliable estimation of the temperature and possibility of zircon crystallization in basic and medium igneous rocks. Using Eq. (4), we calculated the contents of Zr^m necessary for the beginning of zircon crystallization from anhydrous MORB melt at 1 atm (Fig. 5a) and from olivine-normative tholeiitic basalt with an initial water content of 3 wt.% in the temperature range 1170–700 ºC and at 0.7 GPa (Fig. 5b). The diagrams in Fig. 5 were constructed based on the contents of major oxides in the melts at corresponding temperatures (Fig. 5a (Grove et al., 1992) and Fig. 5b (Nandedkar et al., 2014)).

Figure 5a shows that crystallization of zircon from anhydrous MORB melts, even at a near-solidus temperature of 900 ºC, requires a Zr content of 750 ppm, which is several times higher than the Zr contents in basic rocks (100–300 ppm) (Gale et al., 2013). This means that crystallization of zircon phenocrysts during cooling of near-surface (almost anhydrous) basaltic melts is impossible. During deep crystallization of hydrous gabbro, zircon, on the contrary, can form under subliquidus conditions (Fig. 5b). This occurs when the contents of major oxides and Zr in the residual melt correspond to its saturation according to (4). With the fixed major-oxide evolution trend of the melt (marked by gray circles in Fig. 5b) and the specified initial content of Zr (100 ppm), the current temperature (and, accordingly, the degree of melt crystallization), the content of Zr, and the beginning of Zrn crystallization depend on the intensity of Zr accumulation in the melt. Assuming that Zr is virtually absent from the rock-forming magmatic minerals (bulk coefficient of Zr partition between the melt and the minerals, D_{Zr}, is 0.01), we estimate the beginning of zircon crystallization at 830–850 ºC, when the melt fraction is about 25%. When Zr is present in the minerals ($D_{Zr} = 0.7$), zircon saturation is achieved at much lower temperatures (700–730 ºC) and portion of melt (~14%; Fig. 5b).

The above examples show that finding of zircon grains in igneous basic and intermediate rocks must be treated with caution, because they might be not phenocrysts crystallized in parental magma but xenocrysts trapped by magma from lateral rocks during its ascent and eruption. This is especially true for zircons from ultrabasic rocks. In the Russian Geology and Geophysics Journal, there was a discussion about the use of zircon from peridotites and olivine gabbro for dating of geologic processes (Krasnobaev et al., 2019; Dobretsov et al., 2019), which continues the debate of researchers on the genesis of zircons in ultrabasic rocks. In one of the pioneering papers on this problem (Bea et al., 2001), the authors report the crustal origin of zircon and associate its findings in ultrabasic massifs with the continental-crust/mantle recycling. A simpler mechanism (intrusion of thin granitoid veinlets into crustal cold hyperbasic rocks) was proposed by Belousova et al. (2015) based on detailed geochemical studies of zircons from the Tumut ophiolite (Australia). Other researchers, on the contrary, insist that zircon can be a mineral in equilibrium with enstatite and forsterite and that its presence in basic and ultrabasic rocks
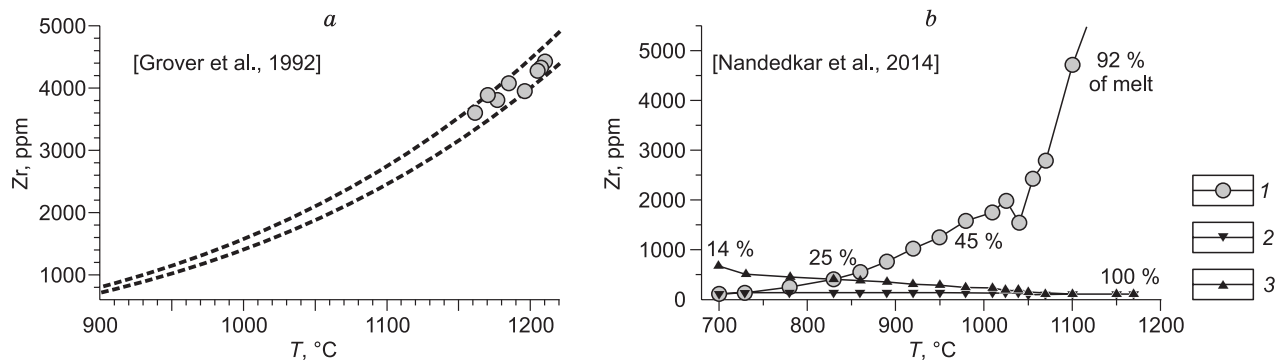

Fig. 5. Solubility of Zr in basic melts (gray circles) crystallizing under anhydrous conditions at 1 atm (*a*) and in the presence of H_2O at 0.7 GPa (*b*) (calculated by Eq. (4)). *1*, solubility of zircon; *2, 3*, lines of Zr accumulation in residual melt, calculated for the initial content Zr = 100 ppm and *D*(melt/Zrn) = 0.7 (*2*) and 0.01 (*3*). The parameters of the line intersection points mark the beginning of Zrn crystallization.

is a natural phenomenon (Krasnobaev and Anfilogov, 2014). We agree with these authors that equilibrium of zircon with solid forsterite and enstatite is possible. This directly follows from the ZrO_2–MgO–SiO_2 phase diagram for 1427 ºC (Pandit and Jacob, 1995). In the absence of phases in which zirconium is a more or less compatible element (e.g., silicate melt and some oxides and silicates (Bea et al., 2006)), zircon or baddeleyite might be stable. Moreover, the mineral form of Zr will be determined by the *P*–*T* parameters and chemical composition of the system. Dobretsov et al. (2019) experimentally showed a complete replacement of zircon by a baddeleyite–olivine mixture in the system MgO–SiO_2–H_2O at 1400 ºC and 2.5 GPa. A very similar result (although with significantly different conclusions) was obtained in experiments in an anhydrous system at 1 atm (Anfilogov et al., 2015). The only difference is that the primary zircon grains were replaced incompletely in the absence of fluid (i.e., with a limited mass transfer) in the latter study. However, equilibrium of zircon with a high-temperature ultrabasic melt with a typical content of Zr (up to 200 ppm (Gale et al., 2013)) is ruled out: The experiments (Borisov and Aranovich, 2019) predict zircon solubility of 5–7 wt.% ZrO_2 under these conditions.

Ti-in-zircon thermometry. The Ti-in-zircon thermometry is one more common method for estimating the temperature of zircon crystallization (Watson and Harrison, 2005; Ferry and Watson, 2007). It is based on experimental calibration of the temperature dependence of the Ti content in **Zrn** in equilibrium with quartz and rutile, which is described by the reaction1

$$TiO_2 + ZrSiO_4 = ZrTiO_4 + SiO_2. \qquad (5)$$
Ru   Zrn   Ti-Zrn   β-Qtz
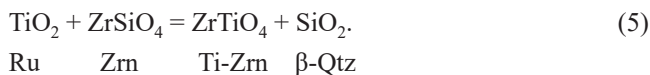
According to Ferry and Watson (2007), who revised the earlier experimental data (Watson and Harrison, 2005), the Ti content (ppm) in Zrn in equilibrium with Ru and Qtz is related to temperature by the equation

$$\lg(\text{Ti, ppm}) = 5.711 - 4800/T, \text{ K}. \qquad (6)$$

If rutile and quartz are absent, it is necessary to introduce a correction for the reduced values of the oxide activities (a_i) into the equilibrium conditions (Ferry and Watson, 2007; Silantyev et al., 2010; Aranovich et al., 2013):

$$\lg(\text{Ti, ppm}) = 5.711 - 4800/T, \text{ K} - \lg(a\text{SiO}_2/a\text{TiO}_2). \qquad (7)$$

Since the reference experiments on the Ti solubility in Zrn were carried out at 10 kbar, correction must also be introduced for rocks formed at significantly different pressures. According to the estimates (Tailby et al., 2011), the volumetric effect of reaction (5) (ΔV (5)) at pressures between 1 atm and 10 kbar is, on average, –1.3 J/(bar·mol); thus, (7) transforms into

$$\lg(\text{Ti, ppm}) = 5.711 - (4800 + 68(P, \text{kbar} - 10))/T, \text{ K} -$$
$$\lg(a\text{SiO}_2/a\text{TiO}_2). \qquad (8)$$

From (8) it follows that even at the same pressures and temperatures, the Ti content in zircon can significantly vary because of the $a\text{SiO}_2/a\text{TiO}_2$ variation in the rock (melt) relative to its saturation with quartz and rutile (in the latter case, $a\text{SiO}_2 = a\text{TiO}_2 = 1$). Significant variations in the Ti contents in zircon grains are often observed (Bin Fu et al., 2008; Ickert et al., 2011).

Let us consider the importance of correct accounting of the varying $a\text{SiO}_2/a\text{TiO}_2$ ratio by the example of a zircon grain from oceanic gabbro (sample I1028-3), considered in detail earlier (Aranovich et al., 2013, Fig. 3, grain 8). The grain core, which has preserved a clear magmatic structure, contains 9.7 ppm Ti, and the porous rim contains 16.3 ppm Ti. The porous zone has fine inclusions of baddeleyite (Bd, ZrO_2). The Zrn + Bd assemblage buffers the SiO_2 activity. The equilibrium curve for the reaction

$$ZrSiO_4 = ZrO_2 + SiO_2, \qquad (9)$$
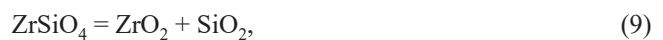
calculated from the thermodynamic data (Berman and Aranovich, 1996; http://twq.petrochronology.org/) at 1 kbar, is given in the temperature–SiO_2 activity coordinates (Fig. 6). The figure also shows equilibrium curves for other reactions indicating the silica activity in basic rocks and the isopleths of the Ti contents in Zrn (ppm) calculated from (8) for specified $a\text{TiO}_2 = 0.4$ (Silantyev et al., 2010). The 15 ppm isopleth crosses the Zrn + Bd equilibrium curve at the point with coordinates of 640 ºC/–0.78 (circle in Fig. 6), which corresponds to the conditions of formation of the outer, hydrothermally altered zones of zircon, containing Bd inclusions. Despite the much lower content of Ti in the unaltered part of the zircon grain, the latter might have crystallized at a much higher temperature if the initial activity of silica in
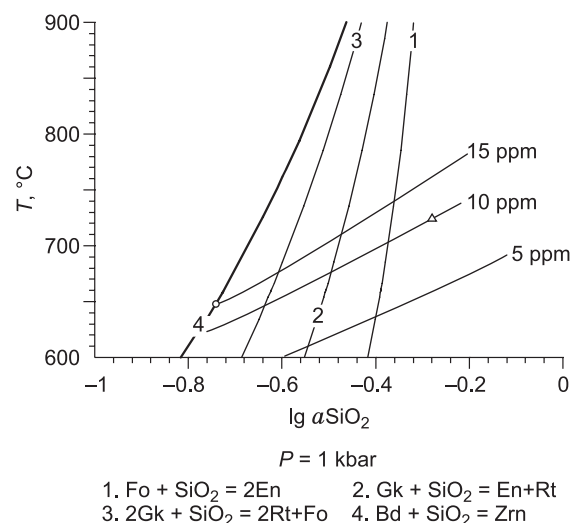

P = 1 kbar

1. Fo + SiO_2 = 2En   2. Gk + SiO_2 = En+Rt
3. 2Gk + SiO_2 = 2Rt+Fo   4. Bd + SiO_2 = Zrn

Fig. 6. Calculated curves for mineral equilibria indicating the silica activity in basic rocks at 1 kbar and the TiO_2 activity of 0.4. Solid monovariant curve marks the reaction Zrn = Bd + SiO_2. Fine curves show the constant activities of end-members (forsterite – 0.77, enstatite – 0.80, geikielite (Gk, $MgTiO_3$) – 0.15). Fine lines are the isopleths of the Ti contents in Zrn (ppm). Also, a curve for the metastable equilibrium of reaction (2) is shown. For explanations, see the text.

the rock was higher (e.g., 730 ºC at lg$a$SiO$_2$ = –0.3, the triangle in Fig. 6). These calculations are approximate, because it is impossible to estimate the pressure and aSiO$_2$/aTiO$_2$ in the above rock sample. Nevertheless, they clearly demonstrate that the Ti-in-Zrn geothermometer must be used with caution, because the variations in Ti contents might be caused not only by temperature but also by other factors, especially when mineral inclusions in zircon mark a drastic change in its growth (dissolution) conditions.

Zr–Hf geothermometer for magmatic zircons. Magmatic zircon usually contains 0.5 to 5 wt.% HfO$_2$ (Hoskin and Schaltegger, 2003), i.e., is a solid solution of zircon and hafnon (Hfn, HfSiO$_4$). Many researchers reported a systematic decrease in Zr/Hf from cores to edges of zircon grains from igneous rocks (Claiborne et al., 2010; Wang et al., 2010; Padilla et al., 2016; Aranovich et al., 2017) and from basic to acid rocks of differentiated continental igneous series (Barth and Wooden, 2010; Claiborne et al., 2010; Padilla et al., 2016). Also, a negative correlation was established between the Zr/Hf ratio and the Ti content approximately indicative of the temperature of zircon crystallization (Grimes et al., 2009; Barth and Wooden, 2010; Claiborne et al., 2010). At first glance, these regular phenomena look paradoxical, because Zr and Hf are elements with very similar crystallochemical properties (the formal charge is +4; the radii of the eight-coordinated ions are 0.83 and 0.84 Å, respectively (Shannon, 1976)) and therefore must weakly fractionate during deep petrogenesis processes (Taylor and McLennan, 1985). These phenomena become clear if one bears in mind that Zr is the most compatible element in zircon during its crystallization from a magmatic melt, i.e., the exchange reaction

$$HfSiO_4 + ZrSiO_4^m = ZrSiO_4 + HfSiO_4^m, \qquad (10)$$
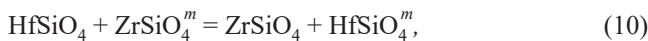
where m is a silicate melt, is significantly shifted to the right. This fact is evidenced from the experimental data on the zircon and hafnon solubility in silicate melts (Ellison and Hess, 1986; Linnen and Kepler, 2002) and on the distribution of Zr and Hf between zircon and melt (Rubatto and Hermann, 2007). The same follows from the partition coefficients of Zr and Hf in the system zircon–silicate melt, predicted by the lattice strain model (Blundy and Wood, 2003).

Exchange reaction (10) meets the following conditions:

$$RT\ln K(10) + \Delta G^o(10) = 0. \qquad (11)$$

The reaction constant is expressed as

$$K(10) = \frac{X_{Zr}^s X_{Hf}^m}{X_{Zr}^m X_{Hf}^s} \cdot \frac{\gamma_{Zr}^s \gamma_{Hf}^m}{\gamma_{Zr}^m \gamma_{Hf}^s} = K_d K_\gamma, \qquad (12)$$

where $K_d = \dfrac{X_{Zr}^s X_{Hf}^m}{X_{Zr}^m X_{Hf}^s}$ is the distribution coefficient of Zr and Hf between Zrn (s) and melt, X_i^j are the molar fractions of the phase components, and K_γ is the product of the activity coefficients (γ_i^j) of the corresponding particles.

Since the crystallochemical properties of Zr and Hf are very similar, we can assume that the Zrn–Hfn solid solution is near-ideal. Even if this is not so, in the narrow range of Hf contents specific to natural magmatic zircons and in the regular-solution approximation, the difference (at T = const)

$$RT(\ln\gamma_{Zr}^s - \ln\gamma_{Hf}^s) = W(X_{Hf}^s - X_{Zr}^s) \approx const, \qquad (13)$$

i.e., the term associated with the nonideal composition of the Zrn–Hfn solid solution, serves as a small correction to $\Delta G^o(10)$ in (11).

The activity coefficients of Zrn and Hfn particles in silicate melts must, on the contrary, differ significantly from unity, as evidenced by the strong dependence of the Zrn and Hfn solubility on the melt composition (Fig. 7). On constructing Fig. 7, we used the melt composition parameter M = (Na + K + 2Ca)/(Al·Si), where the symbols of elements
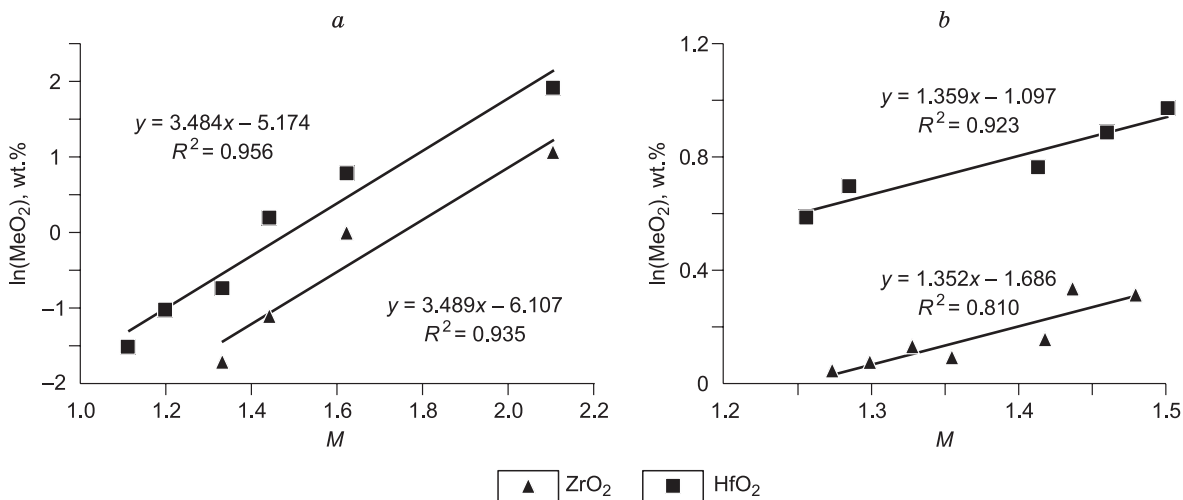

Fig. 7. Dependence of ZrO$_2$ and HfO$_2$ contents (wt.%) on the composition of melts saturated with zircon and hafnon, respectively. *a*, 800 ºC (Linnen and Keppler, 2002); *b*, 1400 ºC (Ellison and Hess, 1986). Linear-dependence equations and correlation coefficients are also given.

mark their mole quantities normalized to the total mole quantity of all elements (Watson and Harrison, 1983; Boehnke et al., 2013). As seen from Fig. 7b, the solubility of both Zrn and Hfn increases by almost an order of magnitude with an increase in M within 1–2. The slopes of the lines, $d(\ln[\text{MeO}_2])/dM$, for ZrO_2 and HfO_2 are almost the same at each T value (Fig. 7a, b), which points to the similar activity coefficients of Zrn and Hfn in aluminosilicate melts. Thus, as a first approximation, we can take $\dfrac{\gamma^m_{\text{Hf}}}{\gamma^m_{\text{Zr}}} = 1$. Then, (11) takes the form

$$RT\ln K_d + \Delta G^{\text{o}*}(10) = 0, \tag{14}$$

where $\Delta G^{\text{o}*}(10)$, in accordance with (10), can differ slightly from the thermochemical value of $\Delta G^{\text{o}}(10)$.

The temperature dependence of $\Delta G^{\text{o}*}(10)$ was calibrated (Aranovich and Bortnikov, 2018) with the use of experimental data on the distribution of Zr and Hf between granite melt and zircon (Rubatto and Hermann, 2007) and on the solubility of Zrn and Hfn in melts of different compositions (Ellison and Hess, 1986; Linnen and Kepler, 2002):

$$\Delta G^{\text{o}*}(10) = -12726 + 7.34T. \tag{15}$$

Substitution of (15) into (14) yields a simple equation for the Zr–Hf geothermometer for Zr-containing igneous rocks:

$$T = \frac{1531}{\ln K_d + 0.883}. \tag{16}$$

As an example, Table 1 presents temperatures estimated with this geothermometer (Eq. (16)) for rock samples from the Austurhorn igneous complex, Iceland (Padilla et al., 2016). In the calculation of Zr/Hf, the content of Zr in zircon was taken constant, $[\text{Zr}] = 480{,}000$ ppm. The calculation results are compared with the temperatures estimated from the zircon saturation index according to (4) (Table 1). The temperatures estimated by the two methods for silica-rich rocks (the samples with the index NS in the table) are in satisfactory agreement. For gabbro (the samples with the index G in the table), the temperatures calculated from the zircon saturation index are underestimated. This discrepancy in temperature values is quite clear: As mentioned above, the bulk composition of basic rocks does not reflect the real composition of the melt from which zircon crystallized at the late stage of differentiation, which results in the lower temperatures estimated from the zircon saturation index. During crystallization of gabbro, much Zr and Hf might have got into rock-forming magmatic clinopyroxene and amphibole and into accessory sphene and ilmenite (Bea et al., 2006). Therefore, the bulk Zr/Hf ratio in the rock might not reflect its value in the melt at the beginning of zircon crystallization.

Fractional crystallization of zircon. According to (14) and (15), the lower the temperature, the greater must be the difference in Zr/Hf between silicate melt and zircon. If this ratio were constant in the melt, zircon crystallizing from the cooling melt should gradually become poorer in Hf. In fact, the Zr/Hf ratio in natural zircons is usually quite opposite: The content of Hf in zircon increases toward the grain edges (Fig. 8) (Claiborne et al., 2010; Aranovich et al., 2017). This is obviously due to a decrease in Zr/Hf in the melt during the fractional crystallization of zircon, which can be described by the Rayleigh fractionation equation

$$C^m = C^{\text{o},m} \times f^{(K_d - 1)}, \tag{17}$$

where C^m and $C^{\text{o},m}$ are the current and initial values of Zr/Hf in the melt and f is the portion of the melt from which zircon crystallizes, $0 \leq f \leq 1$. Note that f not always reflects the true degree of crystallization of silicate melts but often marks only the beginning ($f = 1$) and the end ($f = 0$) of zircon crystallization. Zircon begins to crystallize when it reaches the saturation index (Eq. (4)) depending on both the initial concentration of Zr and the melt composition. Therefore, zircon is an early crystallizing phase in granitic melts (at least in melts of normal alkalinity), whereas in basic melts it crystallizes at the late stages of differentiation, when the true portion of the melt is significantly less than unity. Zircon crystallization can end if Zr is exhausted before the complete solidification of the melt, i.e., when the true portion of the melt is greater than 0.

Figure 9 presents an example of calculation by Eq. (17). As a starting $C^{\text{o},m}$ value, we used the analytical data on the cumulative rock sample BC101-Z (70.84 wt.% SiO_2) from the Spirit Mountain granite batholith, Nevada (Claiborne et al., 2010): $C^{\text{o},m} = 39.55$. Zircons from this sample are highly variable in Hf content and, accordingly, the Zr/Hf ratio (Claiborne et al., 2010). To calculate the initial K_d value in (17), we used the highest $(\text{Zr/Hf})^{\text{Zrn}} = 65.7$ measured in the core of the BC101-2.2C grain (Claiborne et al., 2010). The starting temperature of zircon crystallization, T_0 ($f = 1$), calculated from these compositions by Eq. (16), is 828 ºC. The curves for the composition trends of melt and zircon (solid lines in Fig. 9) were calculated under assumption that the melt fraction f is a linear function of T,

$$f = 1 - k(T - T_0), \tag{18}$$

Table 1. Comparison of temperatures estimated with the Zr–Hf geothermometer (Eq. (16), T, °C) and from the zircon saturation index (Eq. (4), Zrn–T, °C)

Zrn grain	Zr/Hf in rock	Zr/Hf in Zrn	T, °C (16)	Zrn–T, °C
IA-NS-2-4.1	33.01	57.83	787	813
IA-NS-6-2.1	39.48	66.67	815	804
IA-NS-7-15.1	43.41	78.30	766	783
IA-G-1-26.1	35.26	58.14	833	650
IA-G-5-10.1	37.70	73.64	713	697

Note. The sample numbers and analytical data are after Padilla et al. (2016). The Zrn–T values were calculated by Eq. (4).
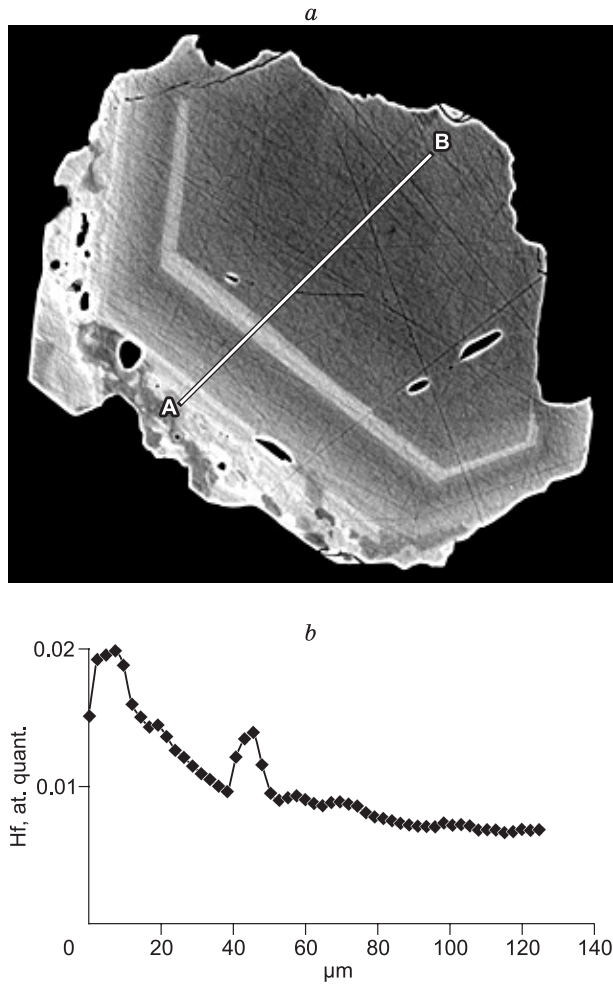
a

b

Fig. 8. BSE images (*a*) and variations in Hf contents (at. quant.) along the A–B profile of zircon grain (*b*) (Aranovich et al., 2016).

and $k = 0.0067$ was evaluated under assumption that $f = 0$ at $T_{fin} = 680$ °C corresponding to the solidus of hydrous granite at 2 kbar (Ebadi and Johannes, 1991). If we use a logarithmic dependence $f(T)$ at the same values of T_0 and T_{fin}, then the position of the curves in Fig. 9 will stay almost unchanged. Since the T_0 value is fixed, the position of the fractionation curves is determined mostly by the k value, which, in turn, depends on T_{fin}. At $T_{fin} = 730$ °C (the solidus of granite at 1 kbar) (Ebadi and Johannes, 1991), k is equal to 0.01, and the composition curves for both phases become steeper (dashed lines in Fig. 9). At $T_{fin} = 650$ °C (the solidus of granite at 3–4 kbar) (Ebadi and Johannes, 1991), k is equal to 0.0056, and the curves become more gentle (dashed lines in Fig. 9). Since the f value for granitoids approximately corresponds to the true melt fraction, construction of curves similar to those in Fig. 9 permits estimation of the final temperature of zircon crystallization. For differentiated rock series, it is also possible to evaluate the temperature at which new portions of melt were separated. For the cumulative-rock sample BC101 from the Spirit Mountain batholith, the lowest Zr/Hf = 32.5 was determined in the zircon grain
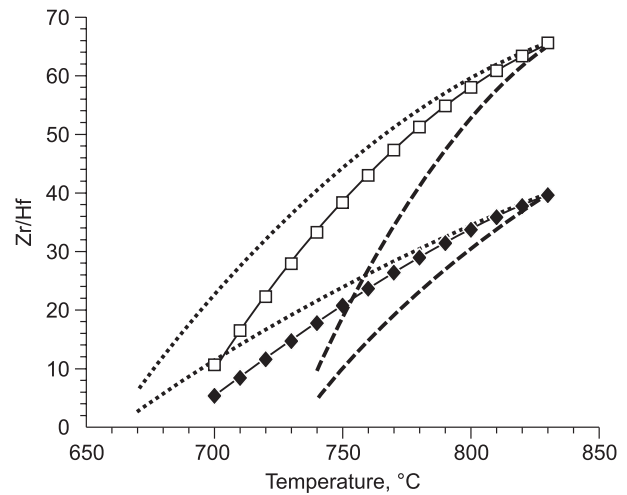

Fig. 9. Zr/Hf trends of zircon (squares) and melt (rhombuses) during the fractional crystallization of zircon from granitoid melt. The compositions of the rock sample BC101-Z and zircons from it (Claiborne et al., 2010) were calculated by Eq. (17) at the initial zircon crystallization temperature $T_0 = 830$ °C and $T_{fin} = 680$ (solid curves), 730 (dashed curves), and 650 °C (dotted curves).

BC101-7.2R (Claiborne et al., 2010). Depending on the chosen k value, this composition corresponds to the final temperature of zircon crystallization of 725–760 °C. In leucogranites, which are the most differentiated fractions of separated melt, Zr/Hf = 23.57 and 20.46 (samples SML49Z and LGZ, respectively) (Claiborne et al., 2010). From the melt differentiation curves in Fig. 9 we estimate that the temperature of melt separation is within 730–780 °C, most likely, within 740–760 °C (curves at $T_{fin} = 680$ °C, $k = 0.0067$). The portion of melt was 0.4–0.5. Note that the initial temperature of crystallization of zircon autocrysts (i.e., grains that crystallized directly from leucogranitic melt) cannot be estimated, because leucogranites contain zircon grains trapped from earlier magmatic intrusive phases (anticrysts) with Zr/Hf ratios close to those of cumulate zircons (Claiborne et al., 2010).

CONCLUSIONS

The studies of the morphology, internal structure, and chemical composition of oceanic zircon show that it is a sensitive indicator of tectonic and physicochemical processes in the lower oceanic crust.

Crystallization of magmatic zircon in gabbroids is not an instantaneous process; it proceeds in the course of differentiation of parental melts in the tectonically active MOR setting. This explains the diversity of its morphological features and deformations and is reflected in the regular variations in its chemical composition both from grain to grain and within individual grains (zoning). The main geochemical indicator of crystallization differentiation during magma cooling is an increase in Hf content toward the zircon grain

edges, which is often accompanied by an increase in the contents of (U + Th) and (Y + P) (Aranovich et al., 2017).

This tendency is also pronounced, but much less, in magmatic zircons from OPG, which is apparently due to the narrower temperature interval of zircon crystallization in these rocks. The OPG zircons are depleted in REE as compared with the least altered magmatic zircons from gabbro, which is probably due to the formation of OPG as a result of the partial melting of gabbro with the participation of a concentrated water–salt fluid, a derivate of seawater (Silantyev et al., 2010; Aranovich et al., 2010, 2013, 2015), and due to the co-crystallization of zircon and apatite.

High-temperature hydrothermal processes within slowly spreading MORs lead to a partial or complete recrystallization of zircon as a result of dissolution/redeposition associated with plastic and brittle strains in the host rocks. The early hydrothermal transformations of zircon are expressed as an increase in its contents of La and other LREE, except for Ce, whose content, on the contrary, decreases as compared with unaltered magmatic zircon. A significantly reduced cerium anomaly and the presence of microinclusions of xenotime, uranium and thorium oxides or silicates, and, sometimes, baddeleyite in zircon alteration zones indicate a reducing type and a high alkalinity of the hydrothermal fluid. The fluid, a derivate of seawater, acquires these features during circulation near the axial zone of ridges as a result of the phase separation in the system H_2O–NaCl and the interaction of the fluid with abyssal peridotites of oceanic core complexes.

The estimated solubility of zircon in basic melts indicates that even near-solidus crystallization of zircon is highly unlikely in anhydrous basaltic melts but is possible in differentiates of deep-seated hydrous basic magmas.

The Ti-in-Zrn geothermometer must be used with caution, because variations in the Ti content in zircon might be controlled not only by temperature but also by other factors, especially when mineral inclusions in zircon testify to a drastic change in its growth (dissolution) conditions.

A geothermometer based on the distribution of Zr and Hf between zircon and rock has several advantages over indicators of the crystallization temperature of magmatic zircon that are based on the zircon saturation index (Watson and Harrison, 1983; Boehnke et al., 2013; Borisov and Aranovich, 2019) and the Ti content in zircon (Ferry and Watson, 2007). It does not depend on the composition of melt and on the correct estimates of the SiO_2 and TiO_2 activity. In addition, reconstruction of the Zr and Hf fractionation trends during crystallization of zircon from granitoid melts makes it possible to evaluate the temperature of separation of more differentiated melt fractions.

REFERENCES

Anfilogov, V.N., Krasnobaev, A.A., Ryzhkov, V.M., Kabanova, L.Ya., Valizer, P.M., Blinov, I.A., 2015. Stability of zircon in dunite at 1400–1550 ºC. Dokl. Earth Sci. 464 (1), 963–966.

Antignano, A., Manning, C.E., 2008. Fluorapatite solubility in H_2O and H_2O–NaCl at 700 to 900 ºC and 0.7 to 2.0 GPa. Chem. Geol. 251, 112–119.

Aranovich, L.Ya., 1991. Mineral Equilibria of Multicomponent Solid Solutions [in Russian]. Nauka, Moscow.

Aranovich, L.Ya., Bortnikov, N.S., 2018. New Zr–Hf geothermometer for magmatic zircons. Petrology 26 (2), 115–120.

Aranovich, L.Ya., Bortnikov, N.S., Serebryakov, N.S., Sharkov, E.V., 2010. Conditions of the formation of plagiogranite from the Markov trough, Mid-Atlantic Ridge, 5º52′–6º02′N. Dokl. Earth Sci. 434 (1), 1257–1262.

Aranovich, L.Ya., Zinger, T.F., Bortnikov, N.S., Sharkov, E.V., Antonov, A.V., 2013. Zircon in gabbroids from the axial zone of the Mid-Atlantic Ridge, Markov deep, 6ºN: Correlation of geochemical features with petrogenetic processes. Petrology 21 (1), 1–15.

Aranovich, L.Ya., Prokofiev, V.Yu., Pertsev, A.N., Bortnikov, N.S., Ageeva, O.A., Bel'tenev, V.E., Borisovsky, S.E., Simakin, S.G., 2015. Composition and origin of a K_2O-rich granite melt in the Mid-Atlantic Ridge, 13º34′ N: Evidence from the analysis of melt inclusions and minerals of the gabbro–plagiogranite association. Dokl. Earth Sci. 460 (2), 174–178.

Aranovich, L.Ya., Bortnikov, N.S., Zinger, T.F., Borisovskiy, S.E., Matrenichev, V.A., Pertsev, A.N., Sharkov, E.V., Skolotnev, S.G., 2017. Morphology and impurity elements of zircon in the oceanic lithosphere at the Mid-Atlantic Ridge axial zone (6º–13º N): Evidence of specifics of magmatic crystallization and postmagmatic transformations. Petrology 25 (4), 339–364.

Barth, A.P., Wooden, J.L., 2010. Coupled elemental and isotopic analyses of polygenetic zircons from granitic rocks by ion microprobe, with implications for melt evolution and the sources of granitic magmas. Chem. Geol. 277, 149–159.

Bea, F., 1996. Residence of REE, Y, Th and U in granites and crustal protoliths: implications for the chemistry of crustal melts. J. Petrol. 37, 521–552.

Bea, F., Fershtater, G.B., Montero, P., Whitehouse, M., Levin, V.Y., Scarrow, J.H., Austrheim, H., Pushkariev, E.V, 2001. Recycling of continental crust into the mantle as revealed by Kytlym Dunite zircons, Urals Mts., Russia. Terra Nova 13, 407–412.

Bea, F., Montero, P., Ortega, M., 2006. A LA-ICP-MS evaluation of Zr reservoirs in common crustal rocks: Implications for Zr and Hf geochemistry, and zircon-forming processes. Can. Mineral. 44, 693–714.

Belousova, E.A., Jimenes, J.M.G., Graham, I., Griffin, W.L., O'Reilly, S.Y., Pearson, N., Martin, L., Craven, S., Talavera, C., 2015. The enigma of crustal zircon in upper-mantle rocks: clues from the Tumut ophiolite, southeast Australia. Geology 43, 119–122.

Berman, R.G., Aranovich, L.Y., 1996. Optimized standard state and solution properties of minerals: I. Model calibration for olivine, orthopyroxene, cordierite, garnet, and ilmenite in the system FeO–MgO–CaO–Al_2O_3–TiO_2–SiO_2. Contrib. Mineral. Petrol. 126 (1–2), 1–24.

Bin, Fu F., Page, F.Z., Cavosie, A.J., Fournelle, J, Kita, N.T., Lackey, J.S., Wilde, S.A., Valley, J.W., 2008. Ti-in-zircon thermometry: applications and limitations. Contrib. Mineral. Petrol. 156 (2), 197–215.

Bischoff, J.L., Pitzer, K.S., 1985. Phase relations and adiabats in boiling seafloor geothermal systems. Earth Planet. Sci. Lett. 75, 327–338.

Blundy, J., Wood, B., 2003. Mineral–melt partitioning of uranium, thorium and their daughters. Rev. Mineral. Geochem. 52, 59–124.

Boehnke, P., Watson, E.B., Trail, D., Harrison, T.M., Schmitt, A.K., 2013. Zircon saturation re-visited. Chem. Geol. 351, 324–334.

Bogdanov, N.A., Dobretsov, N.L., 1987. Ophiolites of California and Oregon. Geotektonika, No. 5, 97–105.

Borisov, A., Aranovich, L., 2019. Zircon solubility in silicate melts: New experiments and probability of zircon crystallization in deeply evolved basic melts. Chem. Geol. 510, 103–112.

Bortnikov, N.S., Savel'eva, G.N., Matukov, D.I., Sergeev, S.A., Berezhnaya, N.G., Lepekhina, E.N., Antonov, A.V., 2005. The zircon age of plagiogranites and gabbros based on SHRIMP data: Pleistocene intrusion in the MAR rift valley, 5º30.6'–5º32.4' N. Dokl. Earth Sci. 404 (7), 1054–1058.

Bortnikov, N.S., Sharkov, E.V., Bogatikov, O.A., Zinger, T.F., Lepekhina, E.N., Antonov, A.V., Sergeev, S.A., 2008. Finds of young and ancient zircons in gabbroids of the Markov Deep, Mid-Atlantic Ridge, 5º54′–5º02.2′ N (Results of SHRIMP-II U–Pb Dating): Implication for deep geodynamics of modern oceans. Dokl. Earth Sci. 421 (1), 859–866.

Burnham, A.D., Berry, A.J., 2012. An experimental study of trace element partitioning between zircon and melt as a function of oxygen fugacity. Geochim. Cosmochim. Acta 95, 196–212.

Ciazela, J., Koepke, J., Dick, H.J.B., Muszynski, A., 2015. Mantle rock exposures at oceanic core complexes along mid-ocean ridges. Geologos 21, 207–231.

Claiborne, L.L., Miller, C.F., Wooden, J.L., 2010. Trace element composition of igneous zircon: a thermal and compositional record of the accumulation and evolution of a large silicic batholith, Spirit Mountain, Nevada. Contrib. Mineral. Petrol. 160 (4), 511–531.

Coleman, R.G., 1977. Ophiolites. Springer-Verlag, Berlin, Heidelberg.

Coleman, R.G., Peterman, Z.E., 1975. Oceanic plagiogranite. J. Geophys. Res. 80, 1099–1108.

Coogan, L.A., Wilson, R.N., Gillis, K.M., MacLeod, C.J., 2001. Near-solidus evolution of oceanic gabbros: Insights from amphibole geochemistry. Geochim. Cosmochim. Acta 65, 4339–4357.

Davis, D.W., Krogh, T.E., Williams, I.S., 2003. Historical development of zircon geochronology. Rev. Mineral. Geochem. 53 (1), 145–181.

de Baar, H.J., Bacon, M.P., Brewer, P.G., 1985. Rare earth elements in the Pacific and Atlantic Oceans. Geochim. Cosmochim. Acta 49, 1943–1959.

Dobretsov, N.L., Zonenshain, L.P., 1985. Comparison of Riphean–Paleozoic ophiolites of northern Eurasia, in: Riphean–lower Paleozoic ophiolites of northern Eurasia [in Russian]. Nauka, Novosibirsk, pp. 181–193.

Dobretsov, N.L., Buslov, M.M., Vernikovsky, V.A., 2003. Neoproterozoic to early Ordovician evolution of Paleo-Asian ocean: implications to the break-up of Rodinia. Gondwana Res. 6, 143–159.

Dobretsov, N.L., Chepurov, A.I., Sonin, V.M., Zhimulev, E.I., 2019. Stability of zircon in the system MgO–SiO$_2$–H$_2$O at 2.5 GPa. Russian Geology and Gophysics (Geologiya i Geofizika) 60 (4), 447–450 (527–531).

Ebadi, A., Johannes, W., 1991. Beginning of melting and composition of first melts in the system Qz–Ab–Or–H$_2$O–CO$_2$. Contrib. Mineral. Petrol. 106 (3), 286–295.

Ellison, A.J., Hess, P.C., 1986. Solution behavior of +4 cations in high-silica melts: petrological and geochemical implications. Contrib. Mineral. Petrol. 94 (3), 343–351.

Ferry, J.M., Watson, E.B., 2007. New thermodynamic models and revised calibrations for the Ti-in-zircon and Zr-in-rutile thermometers. Contrib. Mineral. Petrol. 154 (4), 429–437.

Gale, A., Dalton, C.A., Langmuir, C.H., Su, Y., Schilling, J.-G., 2013. The mean composition of ocean ridge basalts. Geochem. Geophys. Geosyst. 14, 489–518.

Gervasoni, F., Klemme, S., Rocha-Júnior, E.R.V., Berndt, J., 2016. Zircon saturation in silicate melts: a new and improved model for aluminous and alkaline melts. Contrib. Mineral. Petrol. 171 (3), Article 21.

Grimes, C.B., John, B.E., Cheadle, M.J., Mazdab, J.L., Wooden, J.L., Swapp, S., Schwartz, J.J., 2009. On the occurrence, trace element geochemistry, and crystallization history of zircon from in situ ocean lithosphere. Contrib. Mineral. Petrol. 158 (6), Article 757.

Grimes, C.B., Wooden, J.L., Cheadle, M.J., John, B.E., 2015. "Fingerprinting" tectono-magmatic provenance using trace elements in igneous zircon. Contrib. Mineral. Petrol. 170 (5–6), Article 46.

Grove, T.L., Kinzler, R.J, Bryan, W.B., 1992. Fractionation of Mid-Ocean Ridge Basalt (MORB). Geophys. Monograph Ser. 71, 281–310.

Harley, S.L., Kelly, N.M., 2007. Zircon: tiny but timely. Elements 3 (1), 13–18.

Holland, T.J.B., Powell, R., 1998. An internally consistent thermodynamic data set for phases of petrological interest. J. Metamorph. Geol. 16, 309–343.

Hoskin, P.W.O., 2005. Trace-element composition of hydrothermal zircon and the alteration of Hadean zircon from the Jack Hills, Australia. Geochim. Cosmochim. Acta 69, 637–648.

Hoskin, P.W.O., Schaltegger, U., 2003. The composition of zircon and igneous and metamorphic petrogenesis. Rev. Mineral. Geochem. 53, 27–62.

Ickert, R.B., Williams, I.S., Wyborn, D., 2011. Ti in zircon from the Boggy Plain zoned pluton: implications for zircon petrology and Hadean tectonics. Contrib. Mineral. Petrol. 162 (2), 447–461.

Kaulina, T.V., Sinai, M.Yu., Savchenko, E.E., 2011. Metasomatic replacements and isotope ratios in zircon crystals and crystallogenic models. Zapiski VMO 140 (1), 36–48.

Koepke, J., Feig, S.T., Snow, J., Freise, M., 2004. Petrogenesis of oceanic plagiogranites by partial melting of gabbros: an experimental study. Contrib. Mineral. Petrol. 146 (4), 414–432.

Kostitsyn, Yu.A., Belousova, E.A., Bortnikov, N.S., Sharkov, E.V., 2009. Zircons in gabbroids from the axial zone of the mid-atlantic ridge: U-Pb age and ^{176}Hf/^{177}Hf ratio (Results of investigations by the laser ablation method). Dokl. Earth Sci. 429 (1), Article 1305.

Krasnobaev, A.A., Anfilogov, V.N., 2014. Zircons: Implication for dunite genesis. Dokl. Earth Sci. 456 (1), 535–538.

Krasnobaev, A.A., Rusin, A.I., Valizer, P.M., Likhanov, I.I., 2019. Zirconology of the lherzolite block of the natural massif (South Urals). Russian Geology and Geophysics (Geologiya i Geofizika) 60 (4), 435–446 (514–526).

Liati, A., Gebauer, D., Fanning, C.M., 2009. Geochronological evolution of HP metamorphic rocks of the Adula nappe, Central Alps, in pre-Alpine and Alpine subduction cycles. J. Geol. Soc. 166, 797–810.

Linnen, R.L., Keppler, H., 2002. Melt composition control of Zr/Hf fractionation in magmatic processes. Geochim. Cosmochim. Acta 66, 3293–3301.

Lukanin, O.A., Dernov-Pegarev, V.F., 2010. Partitioning of rare earth elements between an aqueous chloride fluid phase and melt during the decompression-driven degassing of granite magmas. Geochem. Int. 48 (10), 961–978.

Manning, C.E., Aranovich, L.Y., 2014. Brines at high pressure and temperature: Thermodynamic, petrologic and geochemical effects. Precambrian Res. 253, 6–16.

McDonough, W.F., Sun, S.-S., 1995. The composition of the Earth. Chem. Geol. 120, 223–253.

Nandedkar, R.H., Ulmer, P., Müntener, O., 2014. Fractional crystallization of primitive, hydrous arc magmas: an experimental study at 0.7 GPa. Contrib. Mineral. Petrol. 167 (6). Article 1015.

Padilla, A.J., Miller, C.F., Carley, T.L., Economos, R.C., Schmitt, A.K., Coble, M.A., Wooden, J.L., Fisher, C.M., Vervoort, J.D., Hanchar, J.M., 2016. Elucidating the magmatic history of the Austurhorn silicic intrusive complex (southeast Iceland) using zircon elemental and isotopic geochemistry and geochronology. Contrib. Mineral. Petrol. 171 (8–9), Article 69.

Pandit, S.S., Jacob, T., 1995. Phase relations in the system MgO–SiO$_2$–ZrO$_2$ at 1700 K. Metal. Mater. Trans. B 26(2), 397–399.

Perchuk, L.L., 1970. Equilibria among Rock-Forming Minerals [in Russian]. Nauka, Moscow.

Pertsev, A.N., Aranovich, L.Y., Prokofiev, V.I., Bortnikov, N.S., Cipriani, A., Simakin, S.S., Borisovskiy, S.E., 2015. Signatures of residual melts, magmatic and seawater-derived fluids in oceanic lower-crust gabbro from the Vema Lithospheric Section, Central Atlantic. J. Petrol. 56, 1069–1088.

Reed, M.J., Candela, P.A., Piccoli, P.M., 2000. The distribution of rare earth elements between monzogranitic melt and the aqueous volatile phase in experimental investigations at 800 ºC and 200 MPa. Contrib. Mineral. Petrol. 140 (2), 251–262.

Reverdatto, V.V., Likhanov, I.I., Polyanskii, O.P., Sheplev, V.S., Kolobov, V.Yu., 2017. The Nature and Models of Metamorphism [in Russian]. Izd. SO RAN, Novosibirsk.

Rubatto, D., 2002. Zircon trace element geochemistry: partitioning with garnet and the link between U–Pb ages and metamorphism. Chem. Geol. 184, 123–138.

Rubatto, D., Hermann, J., 2007. Experimental zircon/melt and zircon/garnet trace element partitioning and implications for the geochronology of crustal rocks. Chem. Geol. 241, 38–61.

Searle, R., 2013. Mid-Ocean Ridges. Cambridge University Press, Cambridge.

Shannon, R.D., 1976. Revised effective ionic radii and systematic studies of interatomic distances in halides and chalcogenides. Acta Crystal. A32, 751–767.

Silantyev, S.A., Aranovich, L.Ya., Bortnikov, N.S., 2010. Oceanic plagiogranites as a result of interaction between magmatic and hydrothermal systems in the slow-spreading mid-ocean ridges. Petrology 18 (4), 369–383.

Skublov, S.G., Berezin, A.V., Mel'nik, A.E., 2011. Paleoproterozoic eclogites in the Salma area, northwestern Belomorian mobile belt: Composition and isotopic geochronologic characteristics of minerals and metamorphic age. Petrology 19 (5), 470–495.

Sobolev, V.S., 1949. Introduction to the Mineralogy of Silicates [in Russian]. Izd. L'vovskogo Universiteta, Lviv.

Tailby, N.D., Walker, A.M., Berry, A.J., Hermann, J., Evans, K.A., Mavrogenes, J.A., O'Neill, H.St.C., Rodina, I.S., Soldatov, A.V., Rubatto, D., Sutton, S.R., 2011. Ti site occupancy in zircon. Geochim. Cosmochim. Acta 75, 905–921.

Taylor, S.R., McLennan, S.M., 1985. The Continental Crust: Its Composition and Evolution. Blackwell, London.

Trail, D., Watson, E.B., Tailby, N.D., 2012. Ce and Eu anomalies in zircon as proxies for the oxidation state of magma. Geochim. Cosmochim. Acta 97, 70–87.

Wang, X., Griffin, W.L., Chen, J., 2010. Hf contents and Zr/Hf ratios in granitic zircons. Geochem. J. 44, 65–72.

Watson, E.B., 1979. Zircon saturation in felsic liquids: experimental results and applications to trace element geochemistry. Contrib. Mineral. Petrol. 70 (4), 407–419.

Watson, E.B., Harrison, T.M., 1983. Zircon saturation revisited: temperature and composition effects in a variety of crustal magma types. Earth. Planet. Sci. Lett. 64, 295–304.

Watson, E.B., Harrison, T.M., 2005. Zircon thermometer reveals minimum melting conditions on earliest Earth. Science 308, 841–844.

Zinger, T.F., Bortnikov, N.S., Sharkov, E.V., Borisovskii, S.E., Antonov, A.V., 2010. Influence of plastic deformations in zircon on its chemical composition: Evidence from gabbroids of the spreading zone of the Mid-Atlantic Ridge, Markov trough, 6° N. Dokl. Earth Sci. 433 (2), 1098–1103.

Editorial responsibility: N.L. Dobretsov